

## Anisotropic scaling contributions to high-order structure functions in high-Reynolds-number turbulence

Susan Kurien and Katepalli R. Sreenivasan

*Mason Laboratory and Department of Physics, Yale University, New Haven, Connecticut 06520*

(Received 3 April 2000)

We make an attempt at obtaining the scaling exponents for the anisotropic components of structure functions of order 2 through 6. We avoid mixing these components with their isotropic counterparts for each order by using tensor components that are entirely anisotropic. We do this by considering terms of the isotropic sector corresponding to  $j=0$  in the SO(3) decomposition of each tensor, and then constructing components that are explicitly zero in the isotropic sector. We use an interpolation formula to compensate for the large-scale encroachment of inertial-range scales. This allows us to examine the lowest order anisotropic scaling behavior. The resulting anisotropic exponents for a given tensorial order are larger than those known for the corresponding isotropic part. One conclusion that emerges is that the anisotropy effects diminish with decreasing scale, although much more slowly than previously thought.

PACS number(s): 47.27.Gs, 47.27.Jv, 05.40.-a

### I. INTRODUCTION

It has recently been recognized [1–3] that finite shear can have a profound effect on the scaling of structure functions. At least two attempts have been made to understand them quantitatively. The attempt made in Ref. [1] used conditional statistics to guide the extraction of shear-free scaling, the conditioning variable being a large-scale velocity representative of shear effects. In Refs. [2] and [3], we considered a more formal—and potentially more powerful—approach. In this approach, the experimentally measured structure functions were considered to be mixtures of the isotropic part, and higher-order anisotropic parts. The isotropic part was extracted by projecting the measured structure functions onto the isotropic sector of the SO(3) decomposition.

Specifically, we considered the well-known second-order structure function tensor

$$S^{\alpha\beta}(\mathbf{R}) = \langle (u^\alpha(\mathbf{x} + \mathbf{R}) - u^\alpha(\mathbf{x}))(u^\beta(\mathbf{x} + \mathbf{R}) - u^\beta(\mathbf{x})) \rangle, \quad (1)$$

where  $u^\alpha$  represents the velocity component in the direction  $\alpha$  and  $\mathbf{R}$  is the separation distance between the two positions where  $u^\alpha$  and  $u^\beta$  are measured. In this expression, we shall represent the vertical axis as direction 1 and the horizontal streamwise direction as 3, in contrast to the usual convention. If the separation vector  $\mathbf{R}$  is in the streamwise direction represented by  $\alpha = \beta = 3$ , we recover the longitudinal structure function. Purely transverse components result when  $\alpha = \beta = 1$  with  $\mathbf{R}$  along the direction 3, or when  $\alpha = \beta = 3$  and  $\mathbf{R}$  is along direction 1. Longitudinal as well as certain transverse components of the structure function were previously studied [1–3] in order to extract their anisotropic scaling behaviors. In general, these functions display a mixture of  $j=0$  (isotropic) and higher-order  $j$  (anisotropic) components of the SO(3) decomposition with a corresponding mixing of the scaling behavior of the different sectors. Our procedure involved fixing the known isotropic exponent  $\zeta_2$  and varying the fit parameters to solve for the unknown lowest-order anisotropic scaling exponent,  $\zeta_2^{(2)}$ , from the  $j=2$  sector. We

thus determined, for the second-order structure function, the scaling behavior of the anisotropic parts in addition to that of the isotropic part. The conclusion was that the anisotropic parts for the second-order had a larger exponent, implying that anisotropy decreases with scale size. These estimates were consistent with classical expectations from dimensional grounds [4].

Though this procedure was successful, it was somewhat unsatisfactory because the unavoidable mixing of the isotropic and anisotropic contributions and the number of variables for which least-square fits had to be performed. The implementation of the procedure became increasingly cumbersome for high-order tensors. In this article we take a new and more direct approach for extracting anisotropic exponents by considering only those tensor components that are explicitly zero in the isotropic sector, so that whatever is measured derives its contribution *entirely* from the anisotropic sector. We can use the present method in principle to examine the anisotropic contribution of tensors of *any* order without requiring the knowledge of the particular mathematical form of the anisotropic sectors of these tensors. This is a considerable advantage theoretically because the high-order tensors are nontrivial to compute; it is an advantage experimentally because, unlike in numerical simulations, one can measure only some components for simple geometric arrangements of probes.

There is also an urgent reason for our interest in the scaling exponents of the anisotropic components. As we have already indicated, a point of interest in turbulence theory is the rapidity with which anisotropic effects of shear decay with decreasing scale size. These effects for passive scalars do not seem to vanish at small scales no matter how high the Reynolds number [5], but it has been generally thought [6] that they vanish for velocity fields in conformity with dimensional expectations. Recent indications from high-order statistics of certain transverse components [7] have cast doubt on this outlook; they suggest that the anisotropic effects do not diminish at any scale for certain high-order moments, even at sufficiently high Reynolds numbers. To explore this issue further, it is necessary to measure scaling exponents

TABLE I. Measured parameters of data sets. The large scale  $L$  is considered to be of the order of the height from the ground.

Height (m)	$\bar{U}_3$ ( $\text{ms}^{-1}$ )	$u'_3$ ( $\text{ms}^{-1}$ )	$10^2\langle\epsilon\rangle$ ( $\text{m}^2\text{s}^{-3}$ )	$\eta$ (mm)	$\lambda$ (cm)	$R_\lambda$	$f_s$ , per channel (Hz)	# of samples per channel
0.11	2.67	0.47	6.6	0.47	2.8	870	5000	$4 \times 10^6$
0.27	3.08	0.48	2.8	0.60	4.4	1400	5000	$4 \times 10^6$
0.54	3.51	0.50	1.5	0.70	6.2	2100	5000	$4 \times 10^6$

associated with anisotropic effects. This is our goal for this article.

In Sec. II we describe the experimental conditions and the data. Section III discusses the manner in which the correct tensor components are identified, and summarizes the results of the analysis. The results obtained in the second-order are in close agreement with the result that  $\zeta_2^{(2)} \approx 4/3$ , obtained previously. (In this article, we are not seeking the accuracy required for obtaining intermittency anomalies in the numerical values of the scaling exponents.) The anisotropic scaling exponents for objects of order 3 through 6 are presented here. The paper concludes with a summary of results in Sec. IV. A tentative conclusion is that the effects of anisotropy do vanish with decreasing scale, albeit more slowly than generally believed.

## II. EXPERIMENTAL CONDITIONS

Three cross-wire probes were arranged at heights of 0.11, 0.27, and 0.54 m above the ground at the Dugway testing site in the Utah desert. The probes are positioned in the strongly sheared part of the boundary layer, normally thought to be the logarithmic region. The ground was level and smooth for upstream distances of the order of a mile, and the measurements, which were made between 6 PM and 9 PM, corresponded to nearly neutral conditions of the atmosphere. The wind conditions were light but steady in direction. The situation can be considered almost comparable to wind-tunnel boundary layers on smooth surfaces. Each probe measured

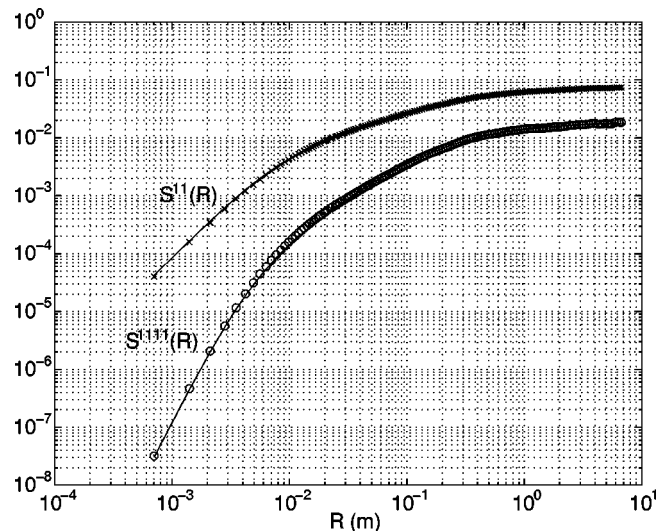


FIG. 1. Log-log plots of transverse structure functions at 0.54 m. X denote the second-order, O, the-fourth order, and the solid lines represent the interpolation fit.

the streamwise and vertical components of the velocity. For each of these heights, Table I shows, among other things, the mean velocities  $\bar{U}$ , root-mean-square fluctuation  $u'_3$  in the streamwise direction 3, the Reynolds number based on the streamwise Taylor microscale, and the mean dissipation rate  $\epsilon$  based on assumptions of local isotropy and Taylor's hypothesis, given by  $\epsilon = 15\nu(\overline{du_3/dx_3})^2$ . In all cases, the turbulence intensity  $u'_3/\bar{U} < 20\%$  which allows us to use Taylor's hypothesis to surrogate time for space, using  $R = U_3 t$  in all that follows.

## III. METHOD AND RESULTS

### A. The second-order structure function

We first consider the second-order tensor  $S^{\alpha\beta}(\mathbf{R})$ . Isotropy implies that this tensor can be expressed as a linear combination of two terms,  $\delta^{\alpha\beta}$  and  $R^\alpha R^\beta$ . As is well known, both terms give nonzero contributions to longitudinal as well as transverse components, corresponding to  $\alpha = \beta$ . For  $\alpha \neq \beta$  these two terms are identically zero if  $\mathbf{R}$  is taken to be in the streamwise direction 3. Therefore, we compute the so-called mixed structure function

$$S^{31}(R) = \langle (u^3(x+R) - u^3(x))(u^1(x+R) - u^1(x)) \rangle, \quad (2)$$

where, as already noted, the superscripts 1 and 3 denote the vertical and streamwise components, respectively. This object is identically zero in the isotropic sector, and so, any

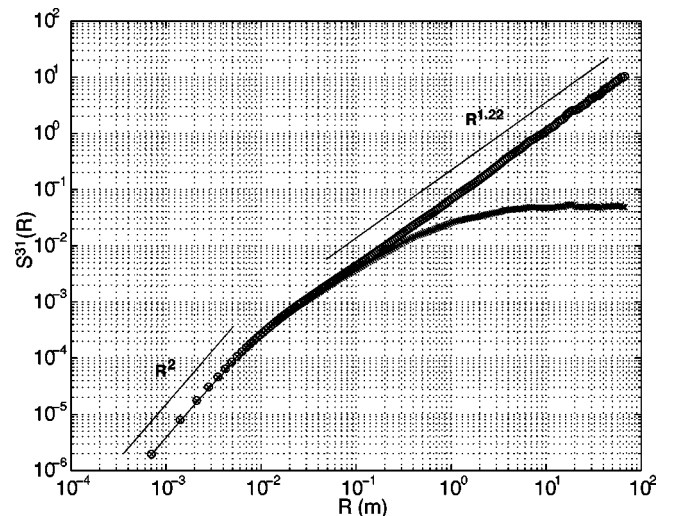


FIG. 2. Log-log plot of second-order mixed structure function at 0.54 m. X denote data, the solid line is the interpolation fit (not visible beyond an  $R$  of  $10^{-1}$  m because of the closely packed symbols), and O correspond to the large-scale compensated function.

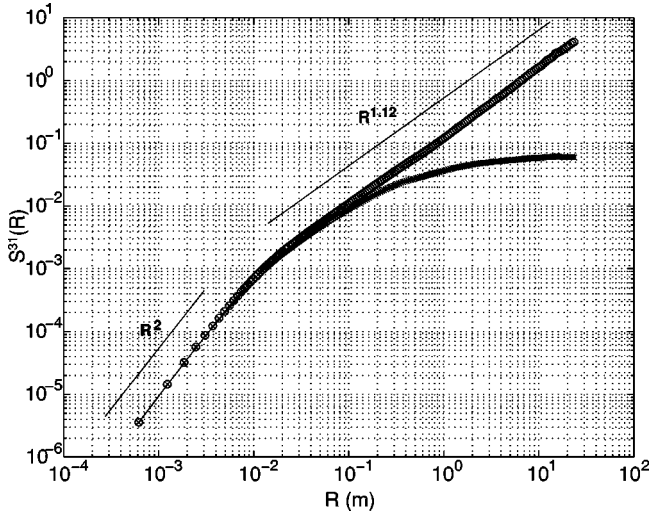


FIG. 3. Log-log plot of second-order mixed structure function at 0.27 m. The legend is the same as for Fig. 2.

scaling behavior that it obeys should come solely from anisotropy. By computing Eq. (2) and examining its scaling, we intend to extract the purely anisotropic scaling behavior in the  $j=2$  sector, uncontaminated by any isotropic scaling, in contrast to the case of either longitudinal or transverse structure functions.

This statement provides us the motivation for examining the measured structure functions  $S^{31}(R)$  at each height. However, as we shall see shortly, apart from the expected  $R^2$  behavior in the dissipative range and saturation at some large scale, there appears to be no distinct inertial range scaling. We suspect that this happens because there is poor scale separation, since the probes are fairly close to the ground; in fact, the large scales (which we expect to be of the order of the height of the probe from the ground and larger [3]) may be encroaching significantly into the inertial range. We would be aided materially in our search for scaling if, somehow, the large-scale effects can be separated. One way of doing this is to write down an interpolation function that models the entire structure function in its three different scaling regions—a dissipative range that scales like  $R^2$  when  $R$  is of the order of the Kolmogorov scale  $\eta$ , a large-scale behavior that tends to saturate (indicating decorrelation) as  $R$  gets to be larger than  $L$ , and the intermediate inertial range for  $\eta \ll R \ll L$  which may exhibit scaling. Through the use of the interpolation formula, one can extract the scaling part in a natural way. This is described below.

A suitable form of the interpolation function is given in

TABLE II. Structure function calculated and the anisotropic scaling exponents for the data at 0.54 m.

Order	$n$	Tensor	$A_n$	$B_n$	$C_n$	$D_n$	$\zeta_n^{(2)} = n - 2C_n$	$\zeta_n$
2	2	$S^{31}$	3.9	0.014	0.39	0.67	1.22	0.7
3	3	$S^{111}$	2400	0.010	0.93	2.28	1.14	1
4	4	$S^{3331}$	5200	0.014	1.21	0.27	1.58	1.26
5	5	$S^{11111}$	$1.22 \times 10^7$	0.029	1.59	3.09	1.82	1.56
6	6	$S^{333111}$	$3.75 \times 10^7$	0.041	1.93	0.50	2.14	1.71

TABLE III. Structure function calculated and the anisotropic scaling exponents for the data at 0.27 m.

Order	$n$	Tensor	$A_n$	$B_n$	$C_n$	$D_n$	$\zeta_n^{(2)} = n - 2C_n$	$\zeta_n$
2	2	$S^{31}$	9.4	0.005	0.44	0.52	1.12	0.7
3	3	$S^{111}$	6940	0.015	0.89	2.78	1.21	1
4	4	$S^{3331}$	$2.1 \times 10^4$	0.014	1.23	0.23	1.54	1.26
5	5	$S^{11111}$	$5.9 \times 10^7$	0.028	1.58	3.52	1.84	1.56
6	6	$S^{333111}$	$2.7 \times 10^8$	0.038	2.00	0.34	2.00	1.71

Ref. [8] for structure functions of arbitrary order. It has the form

$$S^{\alpha_1 \alpha_2 \dots \alpha_n}(R) = \frac{A_n \eta^n (R/\eta)^n}{(1 + B_n (R/\eta)^2)^{C_n}} (1 + D_n (R/L))^{2C_n - n}, \quad (3)$$

where  $A_n$ ,  $B_n$ ,  $C_n$ , and  $D_n$  are variable parameters. This formula is an extension of that given in Ref. [9] and includes a large-scale term. Such extensions have been attempted earlier (e.g., Ref. [10]), but Dhruva [8] has shown that the present interpolation formula works extremely well for longitudinal structure functions of order 2, 4, and 6. To reinforce this point, we test its performance by comparing it to the measured transverse structure function,  $\alpha = \beta = 1$ ,  $R$  in the direction 3. For each data set, the height of the probe is assumed to be the large-scale  $L$ . The fit is shown for the transverse structure function of orders 2 and 4 at the 0.54 m probe in Fig. 1. The comparison between the formula and the data is excellent. Taken together with similar conclusions in [8] for longitudinal structure functions, we conclude that the interpolation formula describes the familiar structure functions very well. For this pragmatic reason, we shall adopt it for our purposes here, and test the robustness of the results obtained in the appendix.

In the formula (3), the large-scale behavior is given by the factor  $(1 + D_2 (R/L))^{2C_2 - 2}$ . If the measured structure function is divided by this factor, we should recover the contri-

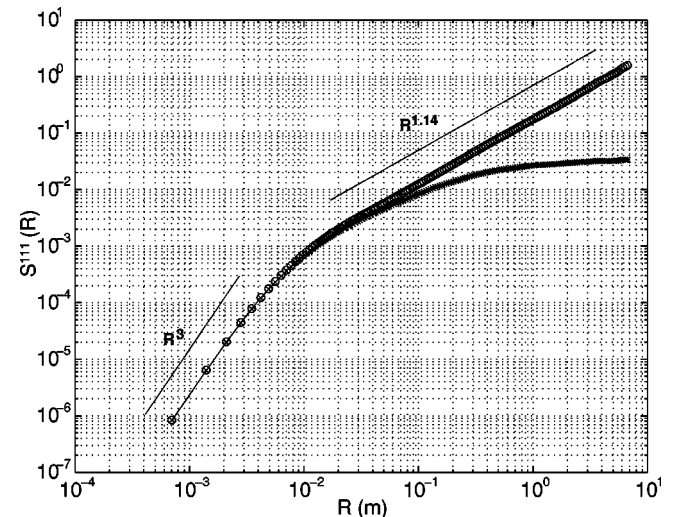


FIG. 4. Log-log plot of third-order transverse structure function at 0.54 m. The legend is the same as for Fig. 2.

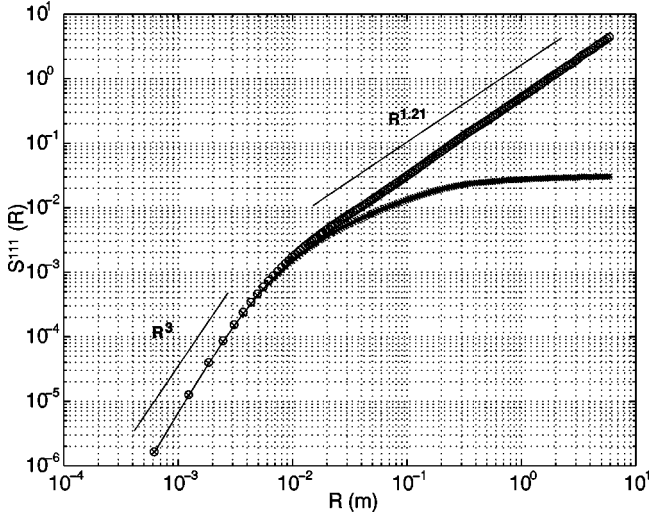


FIG. 5. Log-log plot of third-order transverse structure function at 0.27 m. The legend is the same as for Fig. 2.

bution of the remaining parts—in particular the inertial range part, with the leading order scaling exponent given by  $2 - 2C_2$ .

Figures 2 and 3 display a second-order anisotropic structure function for two heights above the ground. Presumably because of the finiteness of the Reynolds number and the relatively large shear effect, the scaling in the intermediate range  $\eta \ll R \ll L$  is not apparent. However, by dividing out the large-scale contribution as described above, we see two distinct regions of scaling; the dissipative range of  $\sim R^2$  and the extended midrange which scales with exponent between 1.22 and 1.12. The advantage of the scaling function is thus evident: it has allowed us to unequivocally extract a scaling exponent that is most likely to be due to anisotropy. The values of the fitted parameters and the corresponding  $\zeta_2^{(2)}$  are given in Tables II and III for the probes at 0.54 and at 0.27 m, respectively. The error on the measurement of  $C_2$  at 0.54 m is about 0.05 while at 0.27 m it is about 0.08. This gives an error on the estimates of  $\zeta_2^{(2)}$  of 0.07 and 0.11,

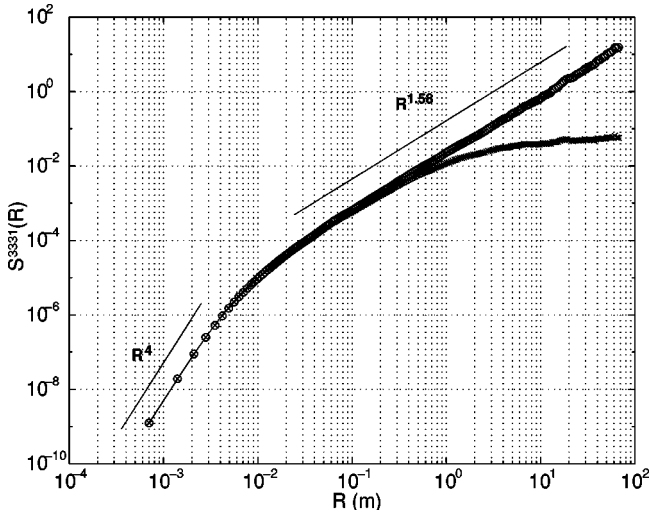


FIG. 6. Log-log plot of fourth-order mixed structure function at 0.54 m. The legend is the same as for Fig. 2.

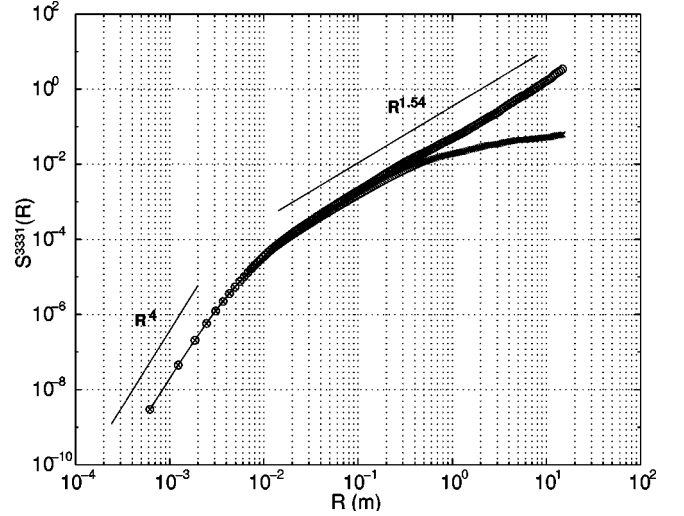


FIG. 7. Log-log plot of fourth-order mixed structure function at 0.27 m. The legend is the same as for Fig. 2.

respectively. This places the theoretically expected value of  $\approx 4/3$  within 1.5 to 2 standard deviations of the present value. This result is consistent with general expectations [4] and the findings of Ref. [2].

### B. Higher-order structure functions

In general, the tensor forms contributing to the  $j=0$  sector for tensors of *any* rank  $n$  are composed of linear combinations of the Kronecker- $\delta$  and the components of  $\mathbf{R}$  along the tensor indices. The following is a list of isotropic tensor contributions for rank 3 through 6:

- (i)  $n=3$ :  $\delta^{\alpha\beta}R^\gamma$  + permutations, and  $R^\alpha R^\beta R^\gamma$ ;
- (ii)  $n=4$ :  $\delta^{\alpha\beta}\delta^{\gamma\delta}$  + permutations,  $\delta^{\alpha\beta}R^\gamma R^\delta$  + permutations, and  $R^\alpha R^\beta R^\gamma R^\delta$ ;
- (iii)  $n=5$ :  $\delta^{\alpha\beta}\delta^{\gamma\delta}R^\mu$  + permutations,  $\delta^{\alpha\beta}R^\gamma R^\delta R^\mu$  + permutations, and  $R^\alpha R^\beta R^\gamma R^\delta R^\mu$ ;

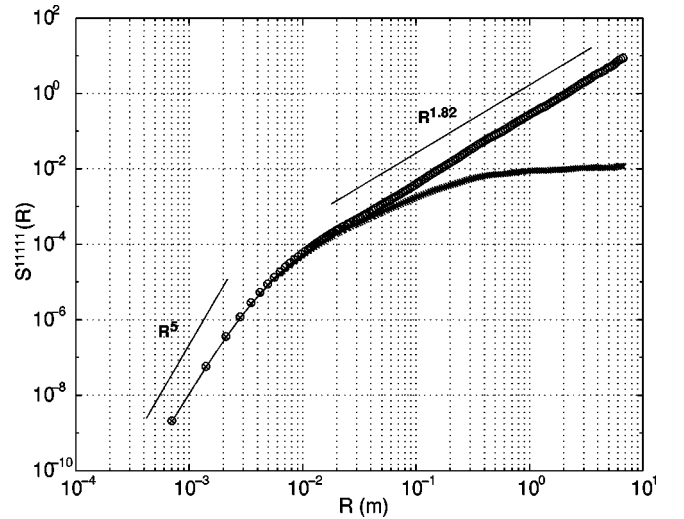


FIG. 8. Log-log plot of fifth-order transverse structure function at 0.54 m. The legend is the same as for Fig. 2.

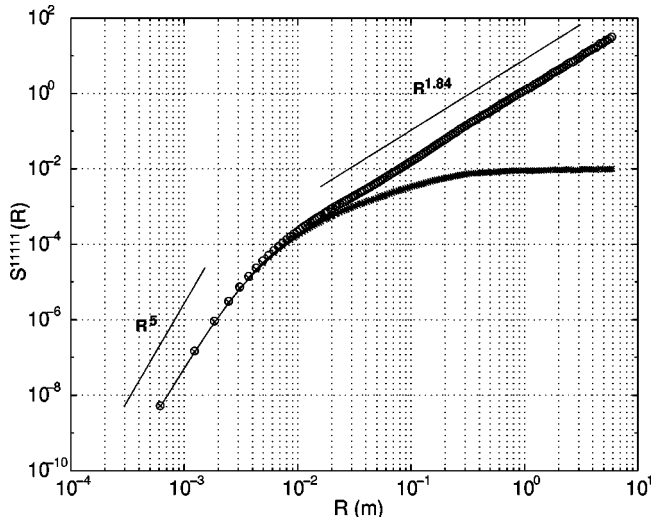


FIG. 9. Log-log plot of fifth-order transverse structure function at 0.27 m. The legend is the same as for Fig. 2.

(iv)  $n=6$ :  $\delta^{\alpha\beta}\delta^{\gamma\delta}\delta^{\mu\nu}$  + permutations,  $\delta^{\alpha\beta}\delta^{\gamma\delta}R^{\mu}R^{\nu}$  + permutations,  $\delta^{\alpha\beta}R^{\gamma}R^{\delta}R^{\mu}R^{\nu}$  + permutations, and  $R^{\alpha}R^{\beta}R^{\gamma}R^{\delta}R^{\mu}R^{\nu}$ .

Based on the above considerations, it can be expected that the structure function components that are zero in the  $j=0$  sector are:

- (i)  $n=3$ :  $S^{111}$  (transverse),  $S^{331}$ ;
- (ii)  $n=4$ :  $S^{3331}$ ,  $S^{3111}$ ;
- (iii)  $n=5$ :  $S^{11111}$  (transverse),  $S^{33111}$ ,  $S^{33331}$ ;
- (iv)  $n=6$ :  $S^{333111}$ ,  $S^{311111}$ ,  $S^{333331}$

Note that the odd-order transverse structure function is *always* zero in the isotropic sector. The functions we shall now consider are given in the second column of Tables II and III. For the case of the third- and fifth-order transverse structure

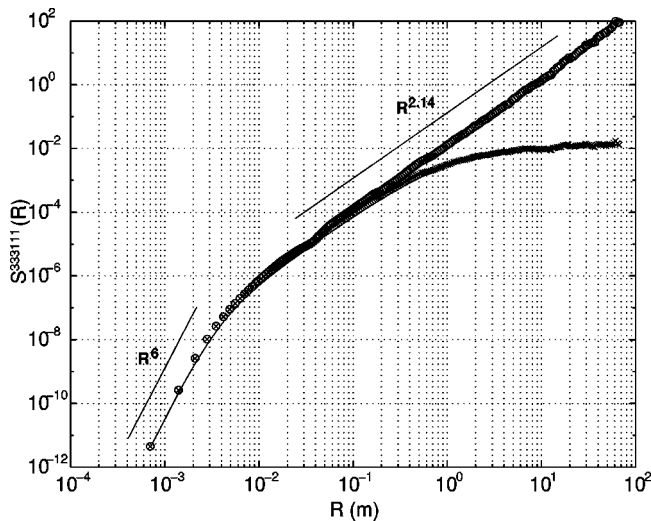


FIG. 10. Log-log plot of sixth-order mixed structure function at 0.54 m. The legend is the same as for Fig. 2.

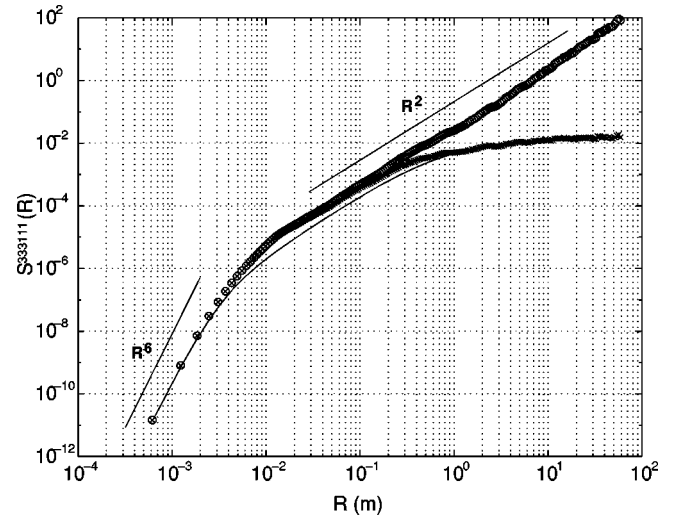


FIG. 11. Log-log plot of sixth-order mixed structure function at 0.27 m. The legend is the same as for Fig. 2.

functions we use the moments of the *absolute value* of the velocity differences in order to obtain better convergence. In using the interpolation function we assume that the inertial range scaling of these anisotropic components is given by a single exponent  $\zeta_n^{(j)}$  where the superscript denotes an isotropic exponent without reference to the precise  $j$ -sector. The compensated functions (with large-scale effects removed) are shown in Figs. 4–11. The errors on the value of  $\zeta_n^{(2)}$  obtained are about 7% at 0.54 m and about 9% at 0.27 m. For comparison, the last column in Tables II and III gives the isotropic scaling exponent of the same order [8]. The entries in this column are measurably smaller than the corresponding nonisotropic exponents. This suggests that the isotropic component alone survives at very small scales.

#### IV. SUMMARY AND CONCLUSIONS

We have presented a method of extraction of anisotropic exponents that avoids mixing with the isotropic sector. We

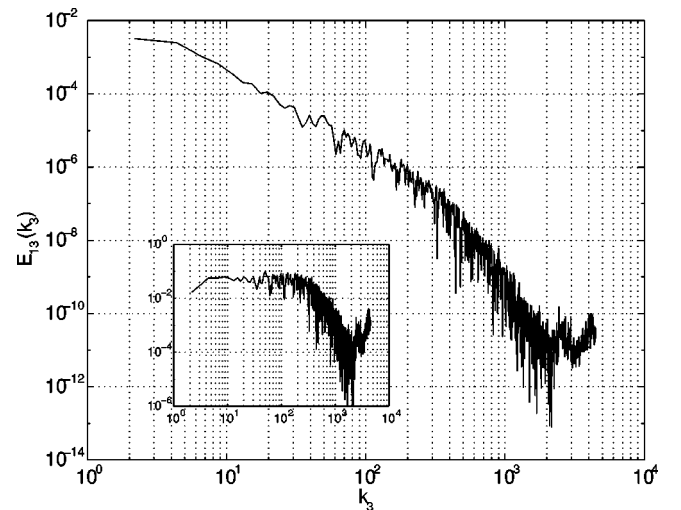


FIG. 12. Log-log plot of the shear-stress cospectrum  $E_{13}(k_3)$  computed at 0.54 m. The inset shows a log-log plot of  $k_3^{2.1} E_{13}(k_3)$  vs.  $k_3$ . The flat region indicates a region of scaling with exponent  $-2.1$ .

TABLE IV. Second-order:  $\zeta_2^{(2)} = 1.25 \pm 0.05$ .

$C_2$	$0.35 \pm 0.1$	$0.35 \pm 0.05$	$0.39 \pm 0.02$	$0.38 \pm 0.05$	$0.38 \pm 0.07$
$\zeta_2^{(2)}$	$1.31 \pm 0.2$	$1.30 \pm 0.10$	$1.21 \pm 0.04$	$1.24 \pm 0.10$	$1.23 \pm 0.14$

do this by explicitly constructing the tensors that are zero in the isotropic sector. An operational step in the extraction of the scaling exponents is the use of an interpolation formula in the spirit of a ‘‘scaling function.’’ This method has allowed us to examine anisotropic effects in structure function tensors of order greater than 2 for the first time. The resulting anisotropic exponents are consistently larger than those known for isotropic parts at all orders. This strongly suggests that anisotropy effects decrease with decreasing scale. However, the rate of decrease is much slower than expected from dimensional arguments (which yield  $4/3$ ,  $5/3$ ,  $2$ ,  $7/3$ , and  $8/3$  for orders 2 through 6).

Our conclusions are based on the use of the interpolation formula, Eq. (3). However, we have shown that the formula works very well in describing the measured structure functions. We have also performed tests of the robustness of the formula by fitting it to smaller sections of the data in order to detect changes in the exponent. A discussion of these checks and their results are presented in the Appendix. To the lowest order, the results are independent of the  $R$ -segment to which the formula is fitted (except, perhaps, when the fit is entirely for the dissipation range or the large-scale range). Any other formula that works equally well will yield similar results. Even so, the formula is empirical, which is why we have not paid much attention to the fact that the scaling exponents obtained for the two probe positions are slightly different, and that the second-order exponent for 0.54 m is slightly larger than that obtained for the third-order. On the whole, the trend is that the exponents become larger for larger orders of the structure function.

The most interesting conclusion of the present work is that the anisotropy effects vanish with decreasing scale more slowly than expected. That anisotropy effects persist at small scales can be seen already at the level of second-order statistics. To illustrate this point, we consider the one-dimensional cospectral density (or shear-stress cospectrum)  $E_{13}(k_3)$ , which is zero in the case of isotropy. From dimensional considerations, the scaling exponent for this object is  $-7/3$  (see Ref. [4]). Figure 12 shows the cospectrum computed for 0.54 m. The inset shows that the cospectrum compensated with a scaling exponent of  $-2.1$  is flat. To the extent that this is numerically smaller than  $7/3$ , the decay of anisotropy is slower than expected, even for second-order quantities. The same conclusion can be drawn from the correlation coefficient spectrum defined by

$$R_{13}(k_3) = \frac{-E_{13}(k_3)}{[E_{11}(k_3)E_{33}(k_3)]^{1/2}}. \quad (4)$$

TABLE V. Third-order:  $\zeta_3^{(2)} = 1.14 \pm 0.11$ .

$C_3$	$0.99 \pm 0.03$	$0.95 \pm 0.04$	$0.88 \pm 0.07$	$0.91 \pm 0.04$	$0.96 \pm 0.08$
$\zeta_3^{(2)}$	$1.01 \pm 0.06$	$1.10 \pm 0.08$	$1.3 \pm 0.14$	$1.2 \pm 0.08$	$1.1 \pm 0.16$

TABLE VI. Fourth-order:  $\zeta_4^{(2)} = 1.61 \pm 0.13$ .

$C_4$	$1.21 \pm 0.07$	$1.12 \pm 0.09$	$1.15 \pm 0.03$	$1.29 \pm 0.1$	$1.21 \pm 0.08$
$\zeta_4^{(2)}$	$1.58 \pm 0.14$	$1.76 \pm 0.18$	$1.7 \pm 0.06$	$1.42 \pm 0.2$	$1.58 \pm 0.16$

To avoid duplication, we simply state the result that this correlation coefficient rolls off at the rate of  $\approx -1/2$  instead of the expected  $-2/3$ . It must be recalled that the dimensional analysis assumes Kolmogorov [11] scaling and therefore does not account for possible intermittency corrections in the anisotropic sectors.

The expectation in the light of the SO(3) formalism is that a hierarchy of increasingly larger exponents, corresponding to increasingly higher-order anisotropic sectors [12], would exist. This expectation appears to have been true in the case of the passively advected vector field [13] where a discrete spectrum of anisotropic scaling exponents is obtained theoretically for all anisotropic sectors. In the present experiments, the fact that the anisotropic effects can be fitted reasonably well by power laws (as seen from Figs. 2–11) suggests that the high-order effects may be small. It is perhaps true, however, that the power laws described here may contain high-order corrections, and that the exponents deduced for the behavior of anisotropy may indeed undergo some revision when contributions from the other sectors of the SO(3) decomposition are also considered. In spite of this possibility, we wish to emphasize that the anisotropy effects for each order of the structure function appear to be well described by something close to a power law with a single exponent. This observation requires further investigation, both theoretically and experimentally. Our main conclusion is that the magnitude of the anisotropic exponents in each order indicate that the falloff from isotropy happens less sharply than previously thought, but that they fall off nevertheless. The higher-order objects considered here have not been studied extensively in the light of anisotropy. We hope that the present experimental results will provide an impetus in this direction.

## ACKNOWLEDGMENTS

We wish to thank Brindesh Dhruva, Christopher White, and Itamar Procaccia for their continued collaboration.

## APPENDIX: TESTS OF THE ROBUSTNESS OF RESULTS

In order to test the robustness of the interpolation formula, we performed the following additional calculations. We considered the data from the probe at the height of 0.54 m. For each order  $n$  of the structure function, we defined a ‘‘window’’ of data extending over two decades of the separation scale,  $R$ . We first placed the lower edge of the window well inside the dissipation range and fit the interpolation formula to the data in the first window. We then moved the lower edge of the window by half a decade and fit the formula to the data in the next window. In this manner, we proceeded until the upper edge of the last window corresponded to the largest value of  $R$ . The entire range of  $R$  yields five windows. We thus obtained five values of the parameter  $C_n$  and calculate the scaling exponent  $\zeta_n^{(2)} = n - 2C_n$  in each case, giving

some indication of the robustness of our result.

Tables IV–VI present the results of performing these checks on structure functions of the second-, third-, and fourth-order. The mean and standard deviation of the exponent values are given in the caption for each table.

It is found that the mean value in each case is in close agreement to the value of the exponents presented in the main text which were obtained by a fit to the entire range of data. This gives us some confidence in the use of the interpolation formula.

- 
- [1] K.R. Sreenivasan and B. Dhruva, *Prog. Theor. Phys. Suppl.* **130**, 103 (1998).  
[2] I. Arad, B. Dhruva, S. Kurien, V.S. L’vov, I. Procaccia, and K.R. Sreenivasan, *Phys. Rev. Lett.* **81**, 5330 (1998).  
[3] S. Kurien, V.S. L’vov, I. Procaccia, and K.R. Sreenivasan, *Phys. Rev. E* **61**, 407 (2000).  
[4] J.L. Lumley, *Phys. Fluids* **10**, 855 (1967).  
[5] K.R. Sreenivasan, *Proc. R. Soc. London, Ser. A* **434**, 165 (1991).  
[6] S. Saddoughi and S. Veeravalli, *J. Fluid Mech.* **268**, 333 (1994).  
[7] S. Garg and Z. Warhaft, *Phys. Fluids* **10**, 662 (1998).  
[8] B. Dhruva, Ph.D. thesis, Yale University, 2000 (unpublished).  
[9] G. Stolovitzky, K.R. Sreenivasan, and A. Juneja, *Phys. Rev. E* **48**, R3217 (1993).  
[10] D. Lohse and A. Muller-Groeling, *Phys. Rev. Lett.* **74**, 1747 (1995).  
[11] A.N. Kolmogorov, *Dokl. Akad. Nauk SSSR* **30**, 301 (1941).  
[12] V.S. L’vov, E. Podivilov, and I. Procaccia, *Phys. Rev. Lett.* **79**, 2050 (1997).  
[13] I. Arad, L. Biferale, and I. Procaccia, *Phys. Rev. E* **61**, 2654 (2000).